

Pulsed laser deposition of SrTiO₃ on a H-terminated Si substrate

Cite this: *J. Mater. Chem. C*, 2013, **1**, 5216

Matjaž Spreitzer,^{*ab} Ricardo Egoavil,^c Jo Verbeeck,^c Dave H. A. Blank^a and Guus Rijnders^a

Interfacing oxides with silicon is a long-standing problem related to the integration of multifunctional oxides with semiconductor devices and the replacement of SiO₂ with high-*k* gate oxides. In our study, pulsed laser deposition was used to prepare a SrTiO₃ (STO) thin film on a H-terminated Si substrate. The main purpose of our work was to verify the ability of H-termination against the oxidation of Si during the PLD process and to analyze the resulting interfaces. In the first part of the study, the STO was deposited directly on the Si, leading to the formation of a preferentially textured STO film with a (100) orientation. In the second part, SrO was used as a buffer layer, which enabled the partial epitaxial growth of STO with STO(110)||Si(100) and STO[001]||Si[001]. The change in the growth direction induced by the application of a SrO buffer was governed by the formation of a SrO(111) intermediate layer and subsequently by the minimization of the lattice misfit between the STO and the SrO. Under the investigated conditions, approximately 10 nm thick interfacial layers formed between the STO and the Si due to reactions between the deposited material and the underlying H-terminated Si. In the case of direct STO deposition, SiO_x formed at the interface with the silicon, while in the case when SrO was used as a buffer, strontium silicate grew directly on the silicon, which improves the growth quality of the uppermost STO.

Received 15th May 2013
Accepted 16th June 2013

DOI: 10.1039/c3tc30913d

www.rsc.org/MaterialsC

Introduction

Interfacing an oxide with silicon is a major challenge and has attracted a great deal of interest from researchers. Solving the problem would enable the epitaxial growth of oxide thin films on a silicon platform, which is very desirable since it represents the core of today's electronics industry. High-quality oxide thin films can provide versatile additional functionalities to the semiconductor industry and can be exploited in high-density magnetic memories, spintronic devices, micro-electro-mechanical systems, and other oxide-based nano-electronic devices.^{1–4} The interfacing problem has mainly been pointed out in studies that investigated the replacement of SiO₂ with high-*k* dielectrics to further scale down the silicon-based devices.⁵

The problem of interfacing both materials is mainly related to the high reactivity of silicon after the native oxide is removed from its surface. This process is required due to the amorphous nature of the native oxide, which hinders the epitaxial growth of the thin film on top of it. Therefore, bare silicon with a defect-free and crystalline surface is most often used as the starting

point for successful film growth. As a result, the deposition process has to be optimized very carefully, and initially oxide-free materials like Sr have to be deposited, which passivate the surface.⁶ On top of it, mainly STO has been grown, because of its high dielectric constant, required for the suitable replacement of SiO₂ in gate oxides, and because of its relatively small lattice mismatch with silicon. The lattice mismatch is 1.7% in the case when the STO is in-plane-rotated by 45° with respect to the silicon. Moreover, epitaxial STO on silicon is also considered as a starting layer for the subsequent overgrowth with different oxides exhibiting many attractive functionalities.

STO on silicon has mainly been grown using molecular beam epitaxy (MBE). The research was pioneered by McKee and his co-workers⁷ and was afterwards much extended by a number of different groups collected in the corresponding ref. 8. Researchers have already managed to successfully grow epitaxial, single-crystal-like STO thin films, even on large 8-inch Si(001) wafers.⁹ The growth process is elaborate and it starts with heating the silicon wafer in an ultra-high vacuum to approximately 980 °C, which results in a clean oxide-free surface.¹⁰ Afterwards, a layer of strontium silicide is formed as a result of the strontium evaporation at 700 °C. This layer protects the silicon from oxidation and enables the epitaxial overgrowth with an oxide. Subsequently, the wafer is cooled below 200 °C, and with the proper evaporation of the strontium in an oxygen atmosphere, three monolayers (MLs) of epitaxial SrO are

^aFaculty of Science & Technology, MESA+ Institute for Nanotechnology, University of Twente, 7500 AE Enschede, The Netherlands

^bAdvanced Materials Department, Jožef Stefan Institute, Jamova 39, 1000 Ljubljana, Slovenia. E-mail: matjaz.spreitzer@ijs.si

^cElectron Microscopy for Materials Research, University of Antwerp, Groenenborgerlaan 171, 2020 Antwerp, Belgium

formed. On top of the SrO, two MLs of amorphous TiO₂ are deposited, which topotactically react with the underlying SrO at 450–550 °C and form epitaxial SrTiO₃. Further growth of the film is achieved by repeated depositions of amorphous SrTiO₃ at low temperatures, followed by crystallization at 450–550 °C. Films prepared by the described procedure are highly crystalline, but contain a number of dislocations, as determined by high-resolution transmission electron microscopy (HRTEM).¹¹ Using post-deposition annealing, the density of the dislocations can be decreased, but only to a certain extent due to the lattice mismatch between the STO and the Si.

Despite the fact that high-quality STO has already been grown on Si, further progress is required in this field since MBE involves a very time-consuming synthesis procedure, while the technique itself is sensitive to the deposition conditions and therefore reproducibility and homogeneity issues are likely to appear during its mass production. In order to avoid these problems, pulsed laser deposition (PLD) was used in our study. In contrast to MBE, the material flux in a PLD process can be tuned over a wide range, which has a major influence on the growth speed. Despite rapid growth, PLD enables the formation of the high-quality epitaxial thin films required from the point of view of applications. Based on a number of samples, Oh and his co-workers determined that homo-epitaxial STO layers prepared using MBE and PLD can exhibit comparable thermal conductivities, which are close to bulk values and indicative of a small number of defects.¹² This was observed in the case when an STO single crystal was used as a PLD target. A second important advantage of PLD is the stability of the process. In contrast to the MBE technique, which operates close to thermodynamic equilibrium, PLD is significantly away from equilibrium. Therefore, minor experimental variations in the deposition conditions do not affect the plume significantly. The deposition and growth remain stable, in line with the requirements for high throughput on an industrial scale.

According to the literature, PLD has already been used in similar studies, including investigations in which different buffer layers, like SrO, CeO₂, and TiN, have been used.^{13,14} In most cases, the native oxide has been removed from the silicon surface using HF and subsequently the substrate has been heated in the PLD chamber in order to evaporate the H atoms from the surface. Such an evaporation of H would result in surface reconstruction under UHV conditions; however, this has not been observed using reflection high-energy electron diffraction (RHEED). Therefore, the exact starting conditions are unclear and could involve an amorphous layer on top of the silicon.

In our work, deposition on a H-terminated surface was performed. The main purpose of this layer was to prevent an extensive reaction between the silicon and the deposited material as its effect has already been demonstrated using MBE.¹⁵ The work is divided into two parts: in the first part, STO was directly deposited, while in the second part, the SrO was used as a buffer, since it is thermodynamically stable in contact with silicon and is thus a favorable candidate for the interface.¹⁶ The main focus of our research was to determine the composition and crystallinity of the interfaces and to correlate them with the deposition conditions. To the best of our knowledge,

the interfaces between the STO or SrO and the H-terminated Si prepared using PLD have not yet been analyzed.

Experimental

The films were grown on 5 mm × 5 mm Si(100) p-type substrates that were cut from the same wafer. Each substrate was first cleaned for 3 minutes in an acetone ultrasonic bath. Afterwards, they were dipped for 3 minutes into a 1% HF solution in order to remove the native oxide from the surface, rinsed with deionised water and introduced into the PLD chamber (Twente Solid State Technology, The Netherlands) within 10 minutes of being removed from the HF solution. Prior to the deposition, the background pressure of the PLD chamber was decreased below 5×10^{-7} mbar. A KrF excimer laser (Coherent, USA, LPX 200, $\lambda = 248$ nm) was used to produce a laser spot size of 2.2 mm² with a fluency of 1.3 J cm⁻². Single-crystalline SrTiO₃ (CrysTec, Germany) and SrO (SurfaceNet, Germany) targets were used and ablated at a repetition rate of 1 Hz. For one ML of STO and SrO, 24 and 32 laser pulses were used, respectively. However, in our study, the actual growth speed was not determined since the RHEED pattern blurred quickly after the deposition started, which was due to the reaction of the deposited material with the underlying substrate. The growth speeds of the STO and SrO mentioned above were determined from the RHEED oscillations observed during the deposition of the material on an STO single crystal and served as a guideline for an estimation of the thin film's thickness. The substrate-to-target distance was set to 5 cm, while the deposition temperature, time and pressure were systematically varied. After the deposition, the films were annealed. They were cooled down to below 150 °C in approximately 250 mbar of pure oxygen at a rate of 10 °C min⁻¹.

X-ray diffraction (XRD) measurements were performed with monochromatic Cu-K α radiation (Bruker AXS, Germany, D8 Discoverer). Using atomic force microscopy (Bruker AXS, Germany, Dimension Icon and Omicron NanoTechnology, Germany, Multimode SPM), the surface morphology of the thin films was analyzed and served for calculations of the surface root-mean-square roughness (R_q). A high-resolution scanning electron microscope (SEM) was used for the microstructural analysis (Carl Zeiss, Germany, Leo 1550). *Ex situ* X-ray photoemission spectroscopy (XPS) was performed using monochromatic Al-K α radiation at a take-off angle of 30° (Physical Electronics, USA, Quantera scanning XPS microprobe).

High-angle annular dark-field (HAADF) scanning-transmission electron microscopy (STEM) and electron energy-loss spectroscopy (EELS) (Fig. 4 and 5) were performed using a FEI Titan microscope operated at 120 kV. The energy resolution for the EELS measurements was 1.25 eV, as determined from the full width at half maximum (FWHM) of the zero-loss peak. The STEM convergence and collection semi-angles used were ~18 mrad and ~173 mrad, respectively. For the HAADF-STEM imaging, an inner detector semi-angle of ~70.4 mrad was used. The quantitative elemental profiles were generated by subtracting a power-law background and integrating the corresponding core-loss excitation edge for each chemical element.

The EELS spectra were analyzed using Digital Micrograph software. To improve the signal-to-noise ratio in the quantitative elemental profiles, principal component analysis was applied to the EELS data sets. High-resolution transmission electron microscope (HRTEM) imaging (Fig. 3 and 11) was performed on a JEOL 3000 transmission electron microscope operated at 300 kV.

Results and discussion

Prior to the deposition, the HF-treated substrates were analyzed using XPS and UHV AFM. The substrates were introduced into the corresponding chamber in about 10 minutes, so that the time of the sample's exposure to air was not shorter than in the case of the deposition. The XPS analysis of the Si 2p peak revealed the presence of the doublet with peaks at 99.2 and 99.8 eV only, which are characteristic for semiconducting silicon. The results did not show the presence of any oxides, such as SiO₂ or SiO_x with peaks at higher binding energies (>103 eV). Before the HF dip, the surface was smooth with an R_q value of 0.04 nm, according to the AFM scan. However, after the removal of the native oxide, R_q increased to 0.13 nm, while the surface remained free of macroscopic defects. In our study, silicon substrates were heated up to 300 °C only before the start of the deposition. Above approximately 550 °C, the hydrogen desorbs from the surface under UHV conditions. As a result, the surface reconstructs, which is a normal starting point for the growth of oxides on Si using MBE. However, in a PLD chamber, the background pressure is usually higher than 10⁻⁶ mbar at temperatures above 550 °C. At such a pressure level, the remaining gas in the vacuum chamber oxidizes the silicon surface and an amorphous layer is formed as a result, which hinders further epitaxial growth. In our study, the initial deposition was set to a low temperature, and therefore, the silicon, which was free of the native oxide, was H protected. Furthermore, the performance of such a protection layer against silicon oxidation was systematically tested.

Direct deposition of STO

In the first part of the study, STO was directly deposited on H-terminated silicon. A number of the deposition parameters had to be carefully optimized in order to control the interfacial reactions and consequently the thickness of the reacted layer. In the optimized case, five MLs of STO were initially deposited at 300 °C in a vacuum (approx. 5 × 10⁻⁷ mbar). These conditions enabled us to slow down the reaction between the deposited material and the silicon. Subsequently, the temperature was increased to 650 °C and the oxygen pressure to 0.01 mbar in order to improve the crystallinity of the film and to decrease the number of oxygen vacancies in the thin film, respectively. Under these conditions, 70 MLs of STO were deposited prior to the annealing. During the first part of the synthesis, the RHEED pattern of the silicon surface blurred and became invisible, indicating the formation of an amorphous layer.

The XRD analysis of the film showed that in addition to the Si(200) peak it is mainly the STO(200) peak that is present in a

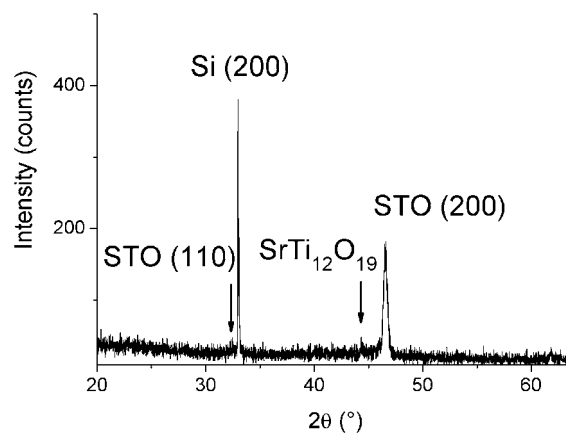


Fig. 1 2Theta-Omega scan of STO directly deposited on H-terminated Si.

2Theta-Omega scan (Fig. 1). In addition, traces of the STO(110) diffraction plane and a SrTi₁₂O₁₉ secondary phase with a peak at $2\theta \approx 44.3^\circ$ were observed as well. Any determination of the secondary phase is nevertheless ambiguous due to the low intensity of the peak and the absence of other diffraction planes in the 2Theta-Omega scan. For the STO(200) peak, FWHM totals 1.8°, according to the omega scan. Furthermore, a Phi scan analysis did not show any in-plane relation between the film and the substrate, indicating that a preferentially textured film was obtained in this part of the study.

The analysis of the microstructure using SEM revealed the presence of polycrystalline grains in addition to a percolative phase (Fig. 2). We anticipate that the latter phase relates to the (100) orientation of the STO, since this orientation is prevailing according to the XRD results, while the polycrystalline grains correspond to the STO with the (110) orientation. According to the AFM analysis, the roughness of the film remains comparable to the H-terminated surface, *i.e.*, $R_q \approx 0.13$ nm. The HRTEM analysis of the film revealed that an interfacial layer with a thickness of about 10 nm was formed between the silicon and STO, having no crystallinity, as already indicated by the RHEED (Fig. 3). The elemental EELS quantification of the corresponding area showed that this layer at the interface corresponds mainly to SiO_x (Fig. 4). However, between the SiO_x and STO, the elemental profiles also show that a layer of silicate formed. The presence of various interfacial layers was also confirmed by high-resolution HAADF STEM, which revealed the

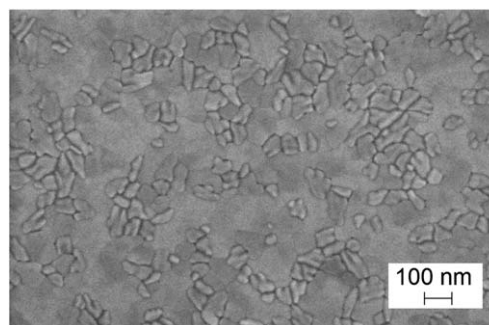


Fig. 2 SEM micrograph of STO directly deposited on H-terminated Si.

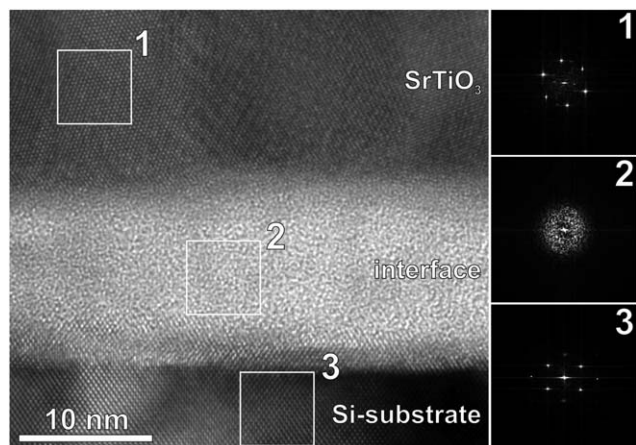


Fig. 3 Left: HRTEM image of STO directly deposited on H-terminated Si. Right: FFT of the respective regions (1, 2 and 3) showing crystallinity of the film and the substrate (1 and 3), as well as the amorphous nature of the interfacial layer (2).

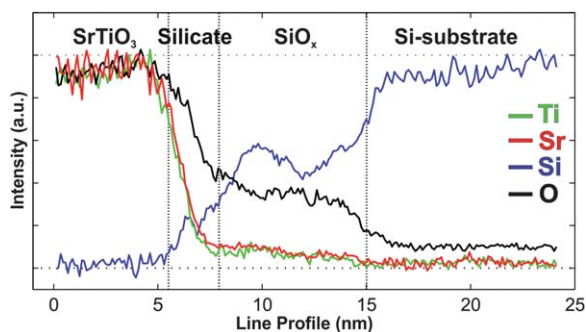


Fig. 4 EELS elemental profiles of Sr-L_{2,3}, Ti-L_{2,3}, Si-K and O-K edges with the STO film (on the left-hand side) and the Si substrate (on the right-hand side).

presence of two layers with different *Z* contrasts between the silicon and the STO (Fig. 5). For the STO layer, the HRTEM and HAADF imaging reveals regions with different orientations, while between them, structural domains and crystalline grain boundaries were observed.

In order to investigate the evolution of the growth, XPS analysis was performed after different deposition periods. For the film with five MLs of STO, which were grown at 300 °C in a vacuum and correspond to the initial part of the synthesis, the analysis of the Si 2p peak revealed that besides the semiconducting silicon a peak at about 101.5 eV is also present in the spectra (Fig. 6). According to the literature data the peak corresponds to a Sr₂SiO₄ silicate.¹⁷ Since the STO was directly deposited on the substrate we anticipate that the compound contains Ti as well, which was indeed confirmed by the presence of a Ti 2p peak and EELS elemental profiles. However, in the literature, there are no corresponding XPS spectra for a proper comparison. After the initial part of the synthesis, 10 MLs of STO were deposited at 650 °C and an oxygen pressure of 0.01 mbar. The XPS results of the film still show a small Si 2p peak at about 101.5 eV. The elemental spectra for other elements (Sr 3d and Ti 2p) correspond well with the data obtained from the STO target, indicating that the STO was

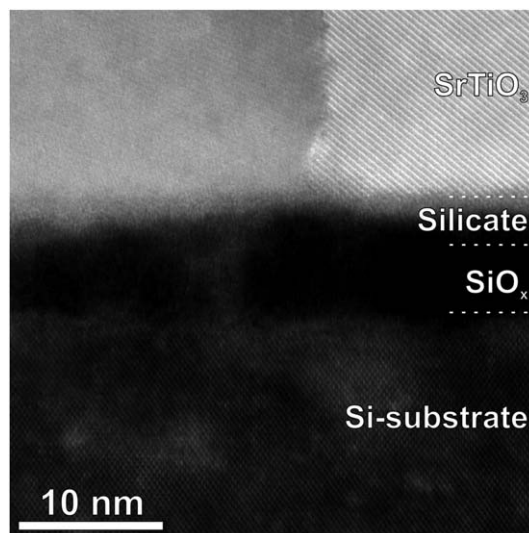


Fig. 5 High-resolution HAADF image showing two different amorphous layers between silicon and STO.

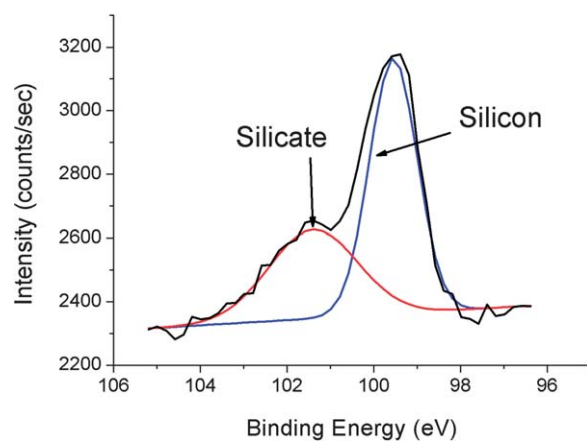


Fig. 6 XPS scan of Si 2p peak for film with 5 MLs of STO directly deposited on Si.

successfully formed on top of the silicate interface. Surprisingly, very similar spectra were obtained for the film with 10 additional MLs of STO, which were deposited again at 650 °C and an oxygen pressure of 0.01 mbar. The presence of the silicate in the latter film, even though it is at a concentration below 1 at%, can be ascribed to the prolonged and thus more intense reaction of the deposited film with the underlying silicon at increased temperature and oxygen pressure. These results indicate that the thickness of the interfacial layer increases with the deposition time and temperature until the silicon becomes thermodynamically more stable and slows down the reaction. Furthermore, the correlation of these results with the TEM analysis reveals that the deposition time and temperature support the formation of a SiO_x layer, which is in direct contact with the underlying silicon. In contrast, the deposition does not affect the thickness of the silicate layer significantly.

In the investigated system, variation of deposition parameters has a significant effect on the growth and structural properties of the as-prepared films. With respect to the optimized

procedure described above, omission of the pre-reaction at 300 °C resulted in the formation of a film with a rougher surface ($R_q \approx 0.22$ nm). The impact on the quality can be related to the removal of the H protection layer, which occurs in a vacuum above 550 °C. Growth in initially high background pressure (at 0.01 mbar) affects the composition of the film with increased concentration of the secondary silicate phase due to pronounced reaction at the interface. In the optimized case the prevailing part of the STO layer was formed at 650 °C and an oxygen pressure of 0.01 mbar. It was observed that the rise in the temperature to 750 °C remarkably increased the concentration of the silicate phase, while the higher pressure environment (0.1 mbar) resulted in the formation of an amorphous layer.

SrO buffer

Since the STO reacted with silicon to a considerable extent, SrO was used as a buffer in the second part of our study. The decision to use SrO was initiated by the thermodynamic study, which among a number of binary compounds identifies only a few compounds that are stable in contact with silicon.¹⁶ Later on, a sharp contact between SrO and Si was also experimentally determined using HRTEM.¹⁸ In contrast, some authors claimed that a silicide⁷ or silicate¹⁹ layer must form at the interface in order to grow an epitaxial STO film on top of the silicon, showing that a final understanding of interfacial chemistry in this investigated system is still not in place.

The growth of SrO on H-terminated silicon was followed by an XPS analysis of the films after different deposition periods, corresponding to the growth of 2, 10, and 20 MLs of SrO. The depositions were performed at 300 °C in a vacuum (approx. 5×10^{-7} mbar) and followed by RHEED. The intensity of the RHEED pattern gradually decreased during the deposition, but in contrast to the direct deposition of the STO, it remained visible after 20 MLs of SrO, even though any intensity oscillations could not be observed. An analysis of the Si 2p peak for the film with two MLs of SrO showed similar results to the film with five MLs of STO, *i.e.*, besides a doublet related to the semiconducting silicon, a peak was observed at 101.5 eV, characteristic of Sr₂SiO₄ silicate. For the film with 10 MLs of SrO, only a silicate peak was observed, which vanished for the 20 MLs SrO film. An analysis of the Sr 3d peak confirmed the presence of a silicate for films with 2 and 10 MLs of SrO, while the film with 20 MLs of SrO showed peaks that were assigned to SrO and SrCO₃ (Fig. 7). The presence of the SrCO₃ carbonate was further supported by an analysis of the C1s peaks. Besides two peaks at 285.0 eV and 286.5 eV, which correspond to C–H and C–O contamination, respectively, a peak at about 291 eV was observed, which was assigned to carbonates. The formation of the carbonate resulted from a fast reaction between the SrO top layer and CO₂ from the air, to which the film was exposed during its transfer from the PLD to the XPS chamber. Our XPS results showed that during the deposition of the SrO on the H-terminated silicon a SrO layer formed only after a relatively thick film of a silicate was formed.

In order to analyze the growth direction of the SrO, a thicker film with 80 MLs of SrO was deposited under the same conditions. Afterwards, the sample was capped with 10 MLs of STO to

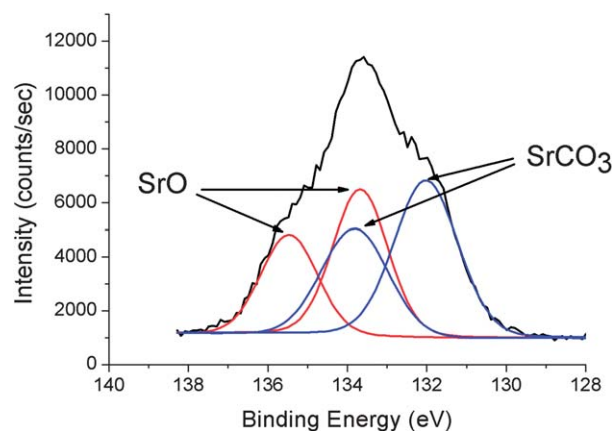


Fig. 7 XPS scan of Sr3d peak for film with 20 MLs of SrO showing deconvolution into two doublets, which correspond to SrO and SrCO₃.

prevent any reaction of the SrO with the CO₂ from the air. The 2Theta-Omega scan of the film revealed only SrO(111) peak in addition to the Si(200) peak, showing only one growth direction of the layer (Fig. 8a).

To understand the growth direction of the SrO, a film with 20 MLs of SrO was prepared. This film served as a buffer, on top of which 75 MLs of STO were deposited. The same conditions as in the above case were used, *i.e.*, the deposition was carried out at 650 °C and an oxygen pressure of 0.01 mbar. A 2Theta-Omega scan of the as-prepared film showed, besides a Si(200) peak, only an STO(110) peak (Fig. 8b). In addition, a Phi scan analysis revealed an in-plane relationship between the STO film and the substrate (Fig. 9). Even though the relationship between the STO(200) peak and the Si(220) peak is weak, it is unambiguous and coincides with the observations of the RHEED pattern after the deposition of the SrO layer. Thus, using the SrO buffer layer, the STO grew epitaxially on the Si with the following orientation relationship: STO(110)||Si(100) (out-of-plane) and STO[001]||Si[001] (in-plane). The same out-of-plane relation between the STO and SrO was already observed in the literature when H-terminated Si(111) was used, with those films being grown using MBE.²⁰ In the above-mentioned work, it was determined that the

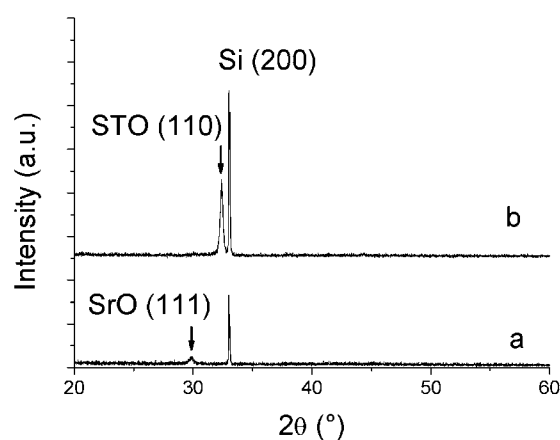


Fig. 8 2Theta-Omega scan of 80 MLs of SrO deposited on H-terminated Si (a) and STO deposited on Si buffered with 20 MLs of SrO (b).

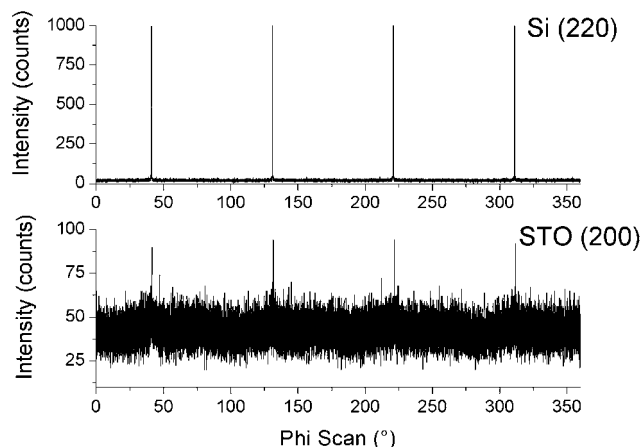


Fig. 9 Phi scan analysis of substrate and STO film deposited on Si buffered with SrO.

STO formed three domains that have an epitaxial relationship with the SrO buffer layer. With respect to the exact domain orientation, the lattice misfit between the STO(110) and SrO(111) is 7.4% or -12.4% . The films were grown at $350\text{ }^{\circ}\text{C}$, while in the case that a higher temperature is used during the synthesis, *i.e.*, $760\text{ }^{\circ}\text{C}$, the STO grows in the (111) direction and exhibits a lattice misfit of 17%. The results of our work correspond to these literature data and indicate that a film with less strain is formed, *i.e.*, with a (110) orientation. However, the main drawback of the as-prepared film is the high value of almost 5° for the FWHM of the STO(110) peak in the omega scan. We believe that this is related to elaborate growth directions of the whole stack, which can be depicted as STO/SrO/Sr₂SiO₄/Si. Since the SrO grew in the (111) direction, this indicates that after the completion of the layer, a surface with oblique crystal planes was obtained. On such oblique planes, the STO was deposited and it grew in the (110) direction. As a result, the straight growth of the STO was hindered, which increased the mosaic spread in the out-of-plane direction, yielding a high value of the FWHM.

A microstructure analysis of the film using SEM revealed that it has a single-phase composition with no inclusions that could be related to crystallites with orientations other than (110). The morphology of the surface showed inclined facets formed due to the (110) growth direction (Fig. 10). Nevertheless, according to the AFM analysis, the surface of the film is smooth, despite the presence of facets, with $R_q \approx 0.07\text{ nm}$. The TEM investigation of the interfacial region revealed that between the silicon and the STO an amorphous layer is present with a thickness of about 12 nm (Fig. 11). Like in the case of the direct deposition of the STO, the interfacial layer consists of two parts (dashed-lines). The EELS spectra showed that a silicate layer is present in contact with the silicon, which is followed by a layer of SrO (Fig. 12). The HRTEM investigation of the film revealed different orientations of the STO grains, with boundaries present between them. Fig. 11 presents the STO with the [111] and [001] orientations on top of silicon that is [011] oriented. The observed [111] orientation of the STO layer is consistent with the XRD results; however, due to the presence of other in-plane orientations, the results showed that the film is not completely epitaxial.

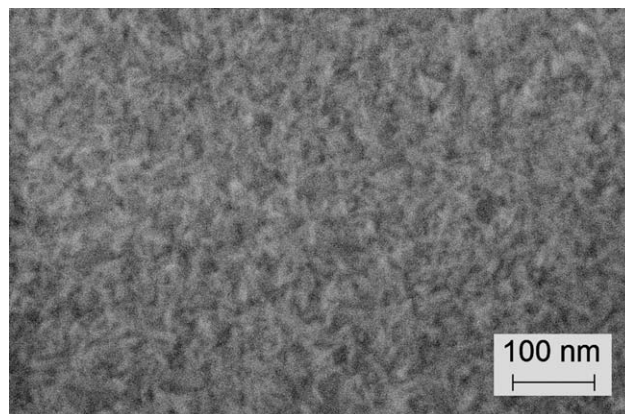


Fig. 10 SEM micrograph of STO deposited on SrO-buffered Si.

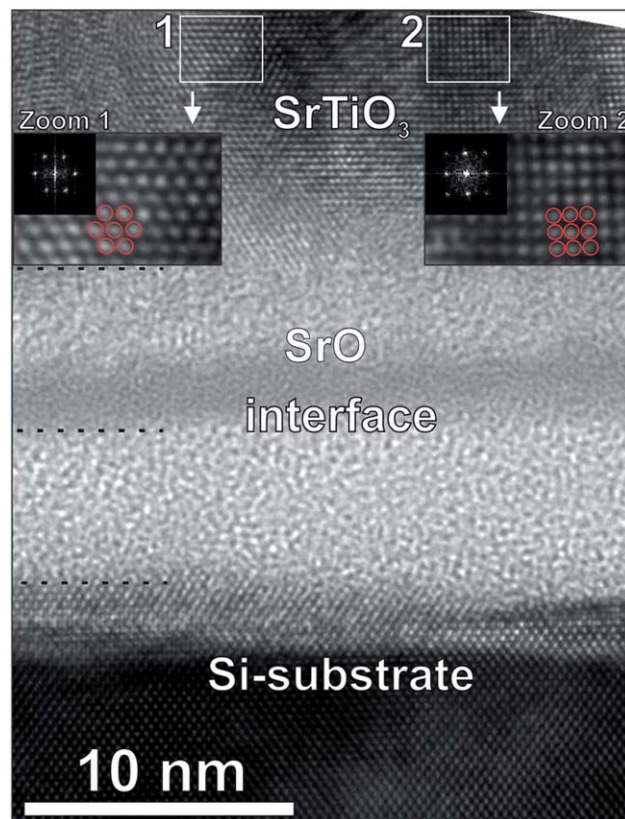


Fig. 11 HRTEM image of STO deposited on SrO-buffered Si substrate. Close-up of the respective regions (1, 2) showing different orientations of the STO layer.

A comparison of the results between both growth methods revealed that at the interface SiO_x and strontium titanium silicate are present in the case of the direct deposition of STO (SiO_x in contact with the silicon), while in the case SrO is first deposited, the interface is composed of strontium silicate and SrO (strontium silicate in contact with the silicon). In the former case, the SiO_x layer prevails, which is mainly due to the thermodynamic instability of the STO with the silicon. In contrast to the STO, the SrO is thermodynamically stable in contact with the silicon, and thus the formation of the reaction layer was not anticipated. However, in our study, the deposited SrO and the silicon reacted

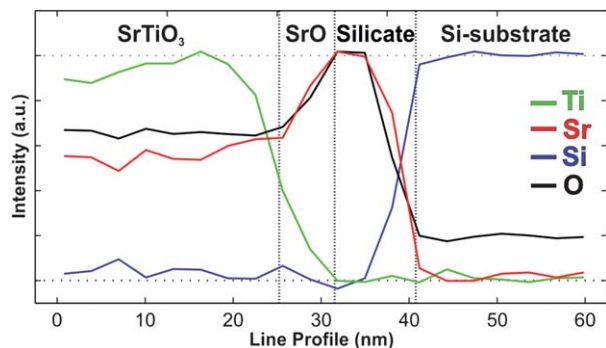


Fig. 12 EELS elemental profiles for STO deposited on SrO-buffered Si substrate. Elemental profiles correspond to Sr-L_{2,3}, Ti-L_{2,3}, Si-K and O-K edges with the STO film (on the left-hand side) and the Si substrate (on the right-hand side). The SrO and silicate layer can be distinct at the interface.

with each other and formed strontium silicate, which is believed to be due to the high energy of the particles during the initial deposition of the SrO in a vacuum. Despite the formation of strontium silicate at the interface, the SrO on top of it grew in the (111) direction, as determined by XRD. The as-prepared layer subsequently serves as a buffer for the overgrowth with STO and is more useful than strontium titanium silicate, which is formed in the case of direct deposition of the STO on the Si.

Conclusions

It was demonstrated that the direct deposition of STO on H-terminated Si resulted in a preferentially textured STO film with a (100) orientation. In the case that SrO was used as a buffer, a partially epitaxial STO film was obtained, while the orientation of the film was changed to (110). The change of the growth direction was governed by the formation of the SrO layer with a (111) orientation and subsequently by the minimization of the lattice misfit between the STO and the SrO. However, under the deposition conditions that were investigated within our study, PLD does not provide full control over the growth of STO, neither for direct deposition, nor in the case of the SrO buffer. Instead of a sharp interface, approximately 10 nm-thick interfacial layers formed between the STO and the silicon due to the reaction between the deposited material and the underlying silicon. The type of interface strongly depends on the deposited material.

Due to the sensitivity of silicon to oxidation, the deposition conditions have a crucial role in the structure of the final interface, which, however, often differs from predictions based on different theoretical models or between different research groups.^{7,10,19,21} Such differences are even more obvious in PLD studies, since the technique involves processes that deviate from thermodynamic equilibrium more than is the case with MBE. In addition, using PLD to interface oxides with silicon has been studied much less extensively than using MBE, and therefore, the growth conditions still remain to be optimized.

Acknowledgements

This work was funded by the European Union Council under the 7th Framework Program grant no. NMP3-LA-2010-246102

I.F.O.X. J.V. acknowledges funding from the European Research Council under the 7th Framework Program – ERC Starting Grant no. 278510 VORTEX.

Notes and references

- 1 A. K. Pradhan, S. Mohanty, K. Zhang, J. B. Dadson, E. M. Jackson, D. Hunter, R. R. Rakhimov and G. B. Loutts, *Appl. Phys. Lett.*, 2005, **86**, 012503.
- 2 R. Bachelet, P. de Coux, B. Warot-Fonrose, V. Skumryev, J. Fontcuberta and F. Sánchez, *J. Appl. Phys.*, 2011, **110**, 086102.
- 3 M. Dekkers, M. D. Nguyen, R. Steenwelle, P. M. te Riele, D. H. A. Blank and G. Rijnders, *Appl. Phys. Lett.*, 2009, **95**, 012902.
- 4 J. Mannhart and D. G. Schlom, *Science*, 2010, **327**, 1607.
- 5 R. A. McKee, F. J. Walker and M. F. Chisholm, *Science*, 2001, **293**, 468.
- 6 Y. Liang, S. Gan, Y. Wei and R. Gregory, *Phys. Status Solidi B*, 2006, **243**, 2098.
- 7 R. A. McKee, F. J. Walker and M. F. Chisholm, *Phys. Rev. Lett.*, 1998, **81**, 3014.
- 8 J. W. Reiner, A. M. Kolpak, Y. Segal, K. F. Garrity, S. Ismail-Beigi, C. H. Ahn and F. J. Walker, *Adv. Mater.*, 2010, **22**, 2919.
- 9 J. W. Park, S. H. Baek, C. W. Bark, M. D. Biegalski and C. B. Eom, *Appl. Phys. Lett.*, 2009, **95**, 061902.
- 10 L. V. Goncharova, D. G. Starodub, E. Garfunkel, T. Gustafsson, V. Vaithyanathan, J. Lettieri and D. G. Schlom, *J. Appl. Phys.*, 2006, **100**, 014912.
- 11 J. W. Park, D. F. Bogorin, C. Cen, D. A. Felker, Y. Zhang, C. T. Nelson, C. W. Bark, C. M. Folkman, X. Q. Pan, M. S. Rzechowski, J. Levy and C. B. Eom, *Nat. Commun.*, 2010, **1**, 94.
- 12 D. W. Oh, J. Ravichandran, C. W. Liang, W. Siemons, B. Jalan, C. M. Brooks, M. Huijben, D. G. Schlom, S. Stemmer, L. W. Martin, A. Majumdar, R. Ramesh and D. G. Cahill, *Appl. Phys. Lett.*, 2011, **98**, 221904.
- 13 O. Nakagawara, M. Kobayashi, Y. Yoshino, Y. Katayama, H. Tabata and T. Kawai, *J. Appl. Phys.*, 1995, **78**, 7226.
- 14 M. B. Lee and H. Koinuma, *J. Appl. Phys.*, 1997, **81**, 2358.
- 15 H. Asaoka, K. Saiki, A. Koma and H. Yamamoto, *Thin Solid Films*, 2000, **369**, 273.
- 16 K. J. Hubbard and D. G. Schlom, *J. Mater. Res.*, 1996, **11**, 2757.
- 17 M. El Kazzi, G. Delhaye, C. Merckling, E. Bergignat, Y. Robach, G. Grenet and G. Hzoellinger, *J. Vac. Sci. Technol., A*, 2007, **25**, 1505.
- 18 S. B. Mi, C. L. Jia, V. Vaithyanathan, L. Houben, J. Schubert, D. G. Schlom and K. Urban, *Appl. Phys. Lett.*, 2008, **93**, 101913.
- 19 C. J. Först, C. R. Ashman, K. Schwarz and P. E. Blöchl, *Nature*, 2004, **427**, 53.
- 20 Y. Macdiha, H. Asaoka, H. Yamamoto and S. Shamoto, *Surf. Sci.*, 2006, **600**, 724.
- 21 L. Fitting Kourkoutis, C. Stephen Hellberg, V. Vaithyanathan, H. Li, M. K. Parker, K. E. Andersen, D. G. Schlom and D. A. Muller, *Phys. Rev. Lett.*, 2008, **100**, 036101.